ACS APPLIED MATERIALS & INTERFACES

www.acsami.org

Research Article

Influence of pH and Surface Orientation on the Photochemical Reactivity of $SrTiO_3$

Mingyi Zhang, Paul A. Salvador, and Gregory S. Rohrer*

Cite This: *ACS Appl. Mater. Interfaces* 2020, 12, 23617−23626

Read Online

ACCESS | Metrics & More | Article Recommendations | Supporting Information

ABSTRACT: The photochemical reactivity of the $SrTiO_3$ surface is affected by the pH of the surrounding aqueous solution. Scanning electron microscopy and atomic force microscopy have been used to quantify the amount of silver that is photochemically reduced on the surfaces of (100), (110), and (111) oriented crystals as a function of pH. For all orientations, the reactivity increases from pH 3, reaches a maximum, and then decreases at higher pH. The pH associated with the maximum reactivity depends on the crystallographic orientation of the surface. The results indicate that the solution pH influences the charge on the $SrTiO_3$ surface. The amount of surface charge influences band bending within $SrTiO_3$, and the maximum reactivity is achieved at a surface charge where neither the photocathodic nor the photoanodic reaction limit the overall reaction rate.

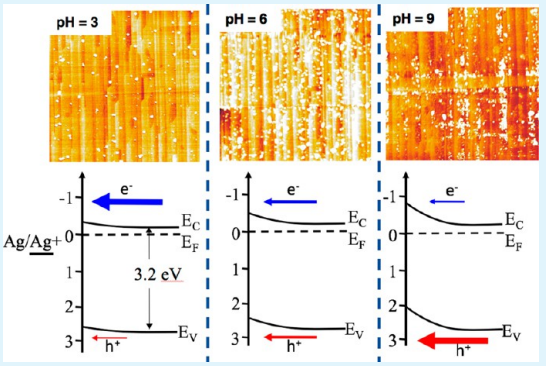

KEYWORDS: *photochemical reactivity, crystallographic orientation, pH, $SrTiO_3$, atomic force microscopy*

INTRODUCTION

Heterogeneous photochemical reactions on semiconductor surfaces have been studied for decades for their potential applications as catalysts for water splitting and the degradation of organic pollutants.[1−5] When photogenerated electrons and holes migrate to semiconductor surfaces, they can drive reduction and oxidation reactions. However, commercial applications are limited by low efficiency.[6,7] Two of the most significant problems are the high rate of photogenerated carrier recombination[8] and the back-reaction of intermediate chemical species.[9] The spatial separation of electrons and holes by internal fields or charged surfaces has been suggested as a potential method to increase the overall photochemical reactivity.[10] For example, a surface domain with a negative (positive) charge will attract holes (electrons) and therefore promote the photoanodic (photocathodic) reaction. As long as the surface contains both photoanodic and photocathodic domains, the overall reaction will be promoted. Internal fields and charged surfaces may arise from phase boundaries,[11,12] ferroelectric polarizations,[13,14] or polar surface terminations.[15,16] Experimental evidence supports the assertion that internal fields and charged surfaces can be used to improve the photochemical reactivity.[17−22]

Because the two half reactions must proceed at the same rate to maintain charge neutrality, the overall reaction rate is limited by the slower one. If one applies a potential to increase the rate of the slower reaction, it will decrease the faster reaction; the maximum overall rate is achieved at a potential where neither of the two half reactions limit the overall rate. For particles in a solution, the potential can be changed by adjusting the pH. The solution pH influences the amount of charge adsorbed on the surface, the surface potential, the band bending in the semiconductor, and, therefore, the concentration of available charge carriers at the surface. Because the photochemical reactivity is directly proportional to the amount of available charge carriers, the pH will affect the overall reaction rate. For example, Zhong et al.[23] made a photochemical water splitting device composed of a $SrTiO_3$ membrane separating solutions of different pH. The gradient in pH created a "chemical bias" so that H_2 was produced on the low pH side of the device and O_2 was produced at the high pH side.

Past studies have shown that pH has a strong influence on the photochemical reaction rate for a variety of catalysts. The effect of pH and the rational for the effect vary with the catalyst and the reaction. Ohtani et al.[24] measured the pH dependence of the photocatalytic activity of TiO_2 powders in silver nitrate solutions from pH 2 to 8. The reactivity is negligible at low pH and increases as the pH increases. The rational provided by the authors was that the positive surface charge at low pH inhibits the adsorption of Ag^+, decreasing the reactivity. The rate of photochemical reduction of Cr^{4+} by TiO_2 decreased as the pH

Received: March 6, 2020
Accepted: April 24, 2020
Published: April 24, 2020

https://dx.doi.org/10.1021/acsami.0c04351
ACS Appl. Mater. Interfaces 2020, 12, 23617−23626

changed from pH 1 to 6, which is opposite what was reported for Ag^+ reduction.[25] Oosawa and Grätzel[26] showed that removing surface OH^- from TiO_2 (presumably making the surface more positive) increased the rate of the oxygen evolution reaction. Guo et al.[27] reported the pH-dependence of photodeposition of a series of metals and metal oxides on faceted BiOBr particles. With increasing pH, there was a reversal of surface charge so that the photocathodic facets became photoanodic and the photoanodic facets became photocathodic.

In the present work, we measure the rate of Ag^+ reduction by $SrTiO_3$ in the range of pH 3 to 9. $SrTiO_3$ is a well-known perovskite photocatalyst that can split water under UV-light illumination.[28−30] $SrTiO_3$ surfaces have the interesting feature of having terraces with different chemical terminations and different electrochemical potentials that have been measured by atomic force microscopy (AFM).[16,31,32] On the (111) and (110) surface, the different potentials lead to photocathodic and photoanodic terraces.[16,32] The reactivities of the terraces with different chemical terminations on the (100) surface have not yet been explored. The presence of photoanodic and photocathodic surface domains on the $SrTiO_3$ surface is analogous to the photoanodic and photocathodic surface domains found on $BaTiO_3$ surfaces because of bulk ferroelectric domains.[14] It has been shown that the rate of Ag^+ photoreduction on $BaTiO_3$ surfaces increases as the pH increases from pH 2 to 8.[33] Song et al.[34] recently showed that hydrogen production from $BaTiO_3/TiO_2$ core/shell photocatalysts varied with pH and exhibited a local maximum in reactivity at pH 9. The rationale for these observations was that increasing negative charge on the surface (with increasing pH) increased upward band bending and increased the rate of the photoanodic reaction, increasing the overall rate of reaction until a maximum is reached; this mechanism is consistent with simulations of the process.[35] In contrast to this earlier work, here we investigate the photochemical reactivity of nonferroelectric, cubic $SrTiO_3$ surfaces. We measure the pH dependence on surfaces of known orientation, because it is known that photochemical reactivity can vary with orientation.[14,36−38]

The purpose of this work is to evaluate the relationship between the solution pH and the photochemical reactivity of three low index $SrTiO_3$ surfaces: (100), (110), and (111). These three facets are commonly found on small catalyst particles,[37,39] and they are also part of the equilibrium shape of $SrTiO_3$ at some temperatures.[40] We use both single crystal surfaces and crystals at the surface of ceramics whose orientations have been measured by electron backscatter diffraction (EBSD). The single crystals show what happens when the surface is almost exclusively a single orientation while the vicinal surfaces identified in the polycrystal show what happens for more realistic surfaces where the principal orientation is combined with smaller facets of other orientations. The photochemical reactivity is determined from topographic AFM images by measuring the volume of silver deposits on the surface after reaction. The observations are then interpreted with a band-bending model. The results imply that to create catalysts with optimized reactivity, it is necessary to control particle shape, chemical termination, and the pH.

EXPERIMENTAL SECTION

The experimental approach is based on photochemical "marker reactions" that leave an insoluble product on the surface at the site of reaction.[14,15,41−43] The reactivity of single crystals, with nearly ideal low index orientations, and grains in a ceramic, with surfaces vicinal to the ideal orientation, were measured as a function of pH and compared. Details of the sample preparation and photochemical marker reactions are given below.

Chemical-mechanical polished (100), (110), and (111) oriented $SrTiO_3$ single crystals (MTI Corporation, Richmond, VA, 0.5 cm × 0.5 cm, roughness <5 Å) were sonicated in a methanol bath for 10 min and then placed in a covered alumina crucible and annealed in a muffle furnace at 1100 °C for 6 h (ramp rates were 5 °C/min). After annealing, atomically flat terraces were observed by AFM (Solver-Next, NT-MDT, Russia). Note that this surface treatment defines a mixed termination that contains both photoanodic and photocathodic terraces.[14,16,32]

Polycrystalline $SrTiO_3$ ceramics were prepared by uniaxially compacting commercially available powder (99%, Alfa Aesar) in a cylindrical dye with a pressure of 150 MPa. A few drops of PVA were added as a binder to form disk-shaped samples with a thickness of 3 mm and a diameter of 1 cm. The samples were placed in an alumina crucible, on top of excess $SrTiO_3$ powder, heated to 900 °C (ramp rates were 5 °C/min) for 12 h to remove any residual organics, sintered for 10 h at 1360 °C (ramp rates were 10 °C/min), and annealed for 6 h at 1470 °C (ramp rates were 10 °C/min) to increase the grain size to about 20 μm. The samples were then cooled in the furnace at a rate of 10 °C/min. The annealed surface was ground with SiC abrasive papers and consecutively polished with a series of diamond suspensions, with a final suspension of 0.25 μm diamond. The polished sample was then annealed at 1150 °C for 6 h to repair polishing damage and thermally etch the grain boundaries. All the heating processes were carried out in air. The crystallographic orientations of individual grains in the polycrystalline sample were determined using an FEI Quanta 200 SEM equipped with an electron backscatter diffraction (EBSD) system. Three grains, close to low index orientations, were selected for comparison to the single crystals.

The photoreduction of aqueous Ag^+ leaves metallic silver on the surface at the site of the reaction. Reaction conditions were selected so that the surface was only partially covered with silver and the underlying surface structure was still obvious so that it was possible to determine the volume of silver. The reaction was carried out using and 10^{-5} M aqueous $AgNO_3$ solution prepared from $AgNO_3$ (Acros) and deionized water. The low concentration was chosen to avoid precipitation.[44] The pH of the solution was controlled through the addition of acetic acid (Fisher Chemical) or NaOH (Acros Organics) and measured using pH test paper (Hydrion). Next, an O-ring was placed on the top of sample and the interior volume was filled with the silver bearing solution. A quartz coverslip was then placed on the top of the O-ring to seal the solution without air bubbles. Next, a 300 W mercury lamp (Newport, Irvine, CA) was used to illuminate the single crystal sample for 30 min. Some single crystal samples were immersed in 10^{-4} M aqueous $AgNO_3$ solution and illuminated for 15 min, which gives a similar distribution of silver deposits. When the polycrystals were reacted using the same conditions as the single crystal, so much silver was deposited that it was not possible to see the underlying surface structure. Because the polycrystal was more reactive than the single crystal, the lamp power was reduced to 150 W and the exposure was reduced to 15 min. After illumination, the pH value of the solution was measured again, and no obvious change was observed. The sample was then rinsed in deionized water and dried using an aeroduster (Miller-Stephenson). Before the next reaction, the sample surface was wiped with cotton swabs and ultrasonically cleaned in methanol and acetone, respectively for 10 min. An XL30 scanning electron microscope (Phillips) was used to make sure that visible deposits were removed. Any amount of Ag that might remain and contaminate the surface is much smaller than what is measured as a product of the reaction. Furthermore, this Ag contamination should be roughly constant throughout the measurements. Unfortunately, a more aggressive cleaning procedure would destroy the surface features that we are using for comparison. After exposure to the entire range of pH, selected experiments were repeated; the results were reproducible, indicating that the surface was not permanently changed by

https://dx.doi.org/10.1021/acsami.0c04351
ACS Appl. Mater. Interfaces 2020, 12, 23617−23626

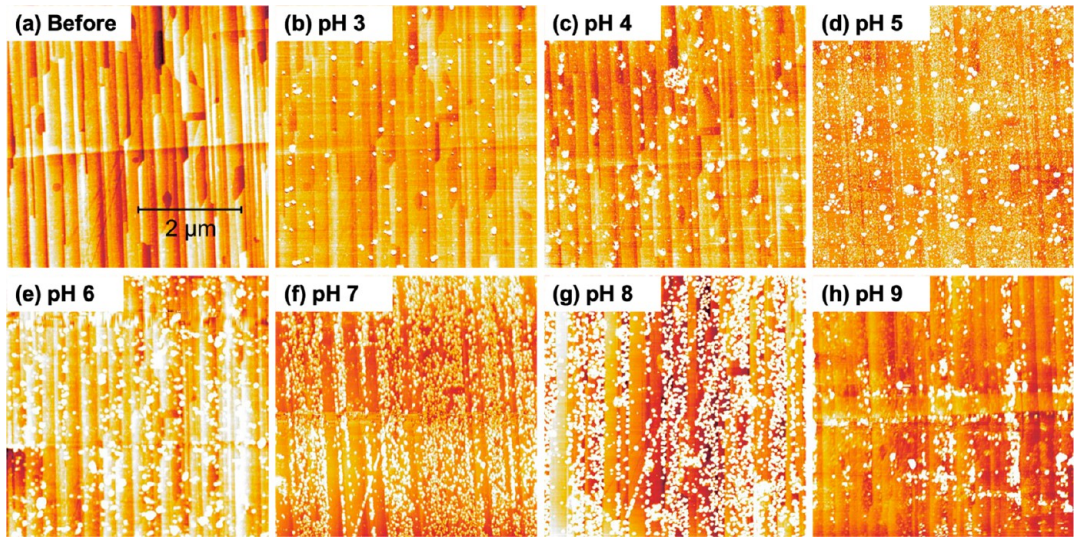

Figure 1. Topographic AFM images of the same location on a (100) $SrTiO_3$ single crystal surface (a) before and (b–h) after photochemical reaction with an aqueous silver nitrate solution having pH values between pH 3–9, as indicated. The dark to light vertical contrast is (a) 1 nm, (b) 20 nm, (c) 20 nm, (d) 20 nm, (e) 40 nm, (f) 10 nm, (g) 5 nm, and (h) 5 nm.

exposure to any of the solutions. For the photooxidation of Pb^{2+}, the sample was immersed in 10^{-3} M aqueous $Pb(CH_3COO)_2$ solution prepared from $Pb(CH_3COO)_2$ (Acros) and deionized water. The lamp was operated at 100 W, and the sample was illuminated for 30 min. All other procedures were the same as for the reduction of Ag^+.

Topographic images of the same area of the surface before and after reaction were obtained by AFM in semicontact mode. The Gwyddion software package,[45] MATLAB, and OriginLab were used to process and analyze the data. To estimate the amount of silver deposited on the surface by the reaction, the images before and after the reaction are compared and the excess volume after the reaction is determined. This is illustrated schematically in Figure S1. The position and height data from the same area before and after the reaction is extracted from the images. To define a constant plane, three points from the clean surface, where no silver is present, are selected in each image (as nearly as possible the same points in each image). A plane is then fit to the three points in each image, and this plane is taken as a reference. Next, the volume is calculated for each image and the excess volume after the reaction is taken to be a measure of the relative amount of silver deposited. For each experiment, the excess volume was measured three times to estimate the variability. To assess tip-related errors, the before images were recorded with three different tips and the results were compared.

RESULTS

A topographic AFM image of the surface of a $SrTiO_3$ (100) single crystal after annealing at 1100 °C in air for 6 h is shown in Figure 1(a). After annealing, the surface is made up of a terrace and step structure, with most steps oriented in the ⟨100⟩ direction. Note that the details of the surface structure depend on the specific surface treatment.[46] The roughness (root-mean-square average of the height profile) of each terrace is less than 1 Å, indicating that they are atomically flat. Topographic AFM images at approximately the same location, after Ag^+ photoreduction at seven different pHs, are shown in Figure 1(b–h). After these reactions, new contrast appeared on the surface, corresponding to reduced metallic silver. Note that the sample was cleaned to remove the silver between each reaction. At pH 3, 4, and 5, the maximum heights of the silver deposits in Figure 1(b–d) are 5 to 15 nm. At pH 6, the maximum heights of the silver deposits in Figure 1(e) are 30 to 40 nm, and at pH 7, 8, and 9, in Figure 1(f–h), they are 5 to 10 nm. Note that the vertical scales of the topographic images in Figure 1 were selected to maximize contrast and vary by a factor of 40. The excess volume of photodeposited silver from pH 3 and pH 9 is illustrated in Figure 2. The mean (circle) and

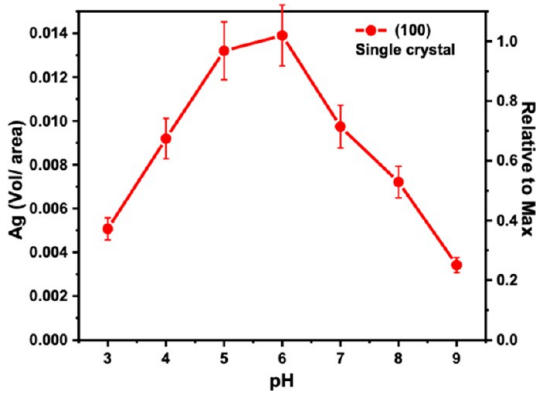

Figure 2. Excess volume of reduced Ag on the $SrTiO_3$(100) surface as a function of pH. Units are μm, computed by dividing the volume (μm^3) by the area (μm^2). The point is the mean and the bars represent the standard deviation from three measurements. The uncertainty in the silver volume is estimated to be 8%. The right-hand vertical axis quantifies the value relative to the maximum value at pH 6.

standard deviation (bars) were determined from three measurements on clean surfaces without reactions. The combined uncertainties based on three different tips and three different sampling areas are estimated to be 8%. Both the changes in the heights of the silver deposits and the excess volume show that the amount of reduced silver increases from pH 3 to pH 6 and then decreases at higher pH. When control experiments were conducted with no light exposure, no silver was found on the surface, verifying that the silver was photoreduced and did not simply precipitate from the solution.

Figures 1(e–g) shows that in the pH range of 6 to 8, the silver deposits in a spatially selective fashion, preferring some terraces over others. This selectivity, not obvious at higher or lower pH, may be related to the fact that $SrTiO_3$(100) surfaces

https://dx.doi.org/10.1021/acsami.0c04351
ACS Appl. Mater. Interfaces 2020, 12, 23617–23626

can be terminated by a TiO_2 or SrO plane.[47] In a more limited study of silver reduction on $SrTiO_3$(100) at uncontrolled pH, this selectivity was not observed.[15] However, terrace-dependent spatial selectivity of reactions on the $SrTiO_3$ (110) and (111) surfaces, and their correlation to the sign of the charge associated with the chemical termination, is well documented.[15,16,32] On the $SrTiO_3$ (110) and (111) surfaces, the differently charged terraces separately promote the photocathodic and photoanodic reactions. To see if this occurs in the same way for the (100) surface, we compared the photocathodic and photoanodic reaction on the same area and the results are illustrated in Figure 3. Note that different conditions

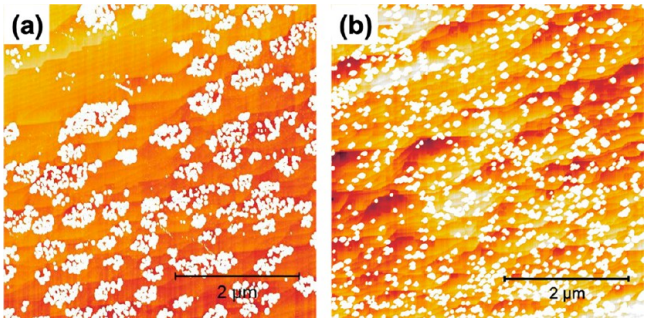

Figure 3. (a and b) Topographic AFM images of the same location on a $SrTiO_3$ (100) crystal after the reduction of silver and the oxidation of lead. The sample in a has been immersed in neutral 10^{-4} M $AgNO_3$ solution and illuminated under 40 W UV light for 15 min, and the sample in b has been immersed in neutral 10^{-3} M $Pb(CH_3COO)_2$ solution and illuminated under 100 W UV light for 30 min.

were used for the two reactions because the photoanodic reaction is much slower than the photocathodic reaction. The image in Figure 3a illustrates that silver is reduced on only some terraces. Compared to Figure 1, these terraces have a different orientation and step spacing, but the reduced silver is clearly localized to certain areas. However, the image in Figure 3b shows a more homogeneous distribution of small Pb-containing particles on the surface. Therefore, all terraces are somewhat photoanodic, but only some are photocathodic at unadjusted pH (pH 6). The bifunctionality of the (100) is consistent with previous findings.[39]

An experiment parallel to the one described above was conducted on the $SrTiO_3$ (110) single crystal surface, and the results are shown in Figure 4. The topographic AFM images show the same area (a) before reaction and (b–h) after reaction in aqueous $AgNO_3$ solutions with pH 3 to 9. The (110) surface consists of (110) terraces with straight step edges; the long step edges have the [001] orientation. As in Figure 1, the bright contrast corresponds to silver deposits, and at some values of pH, silver accumulates mainly along the [001] steps. A qualitative comparison of the topographic images suggests that both the number of silver particles and their heights increase with the pH value from pH 3 to 7 and then decrease at pH 8 and 9. The measurements of the excess volume shown in Figure 5 are consistent with the qualitative

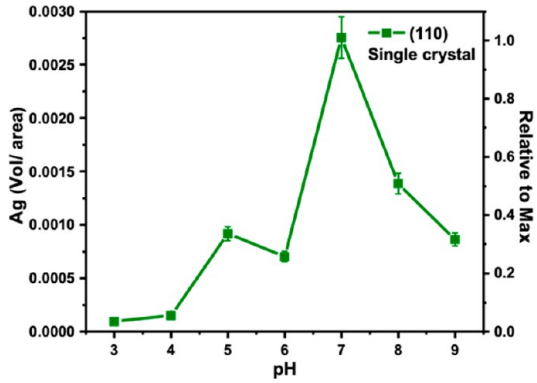

Figure 5. Excess volume of reduced Ag on the $SrTiO_3$(110) surface as a function of pH. Units are μm, computed by dividing the volume (μm^3) by the area (μm^2). The uncertainty in the silver volume is estimated to be 6%. The point is the mean and the bars represent the standard deviation from three measurements. The right-hand vertical axis quantifies the value relative to the maximum value at pH 7.

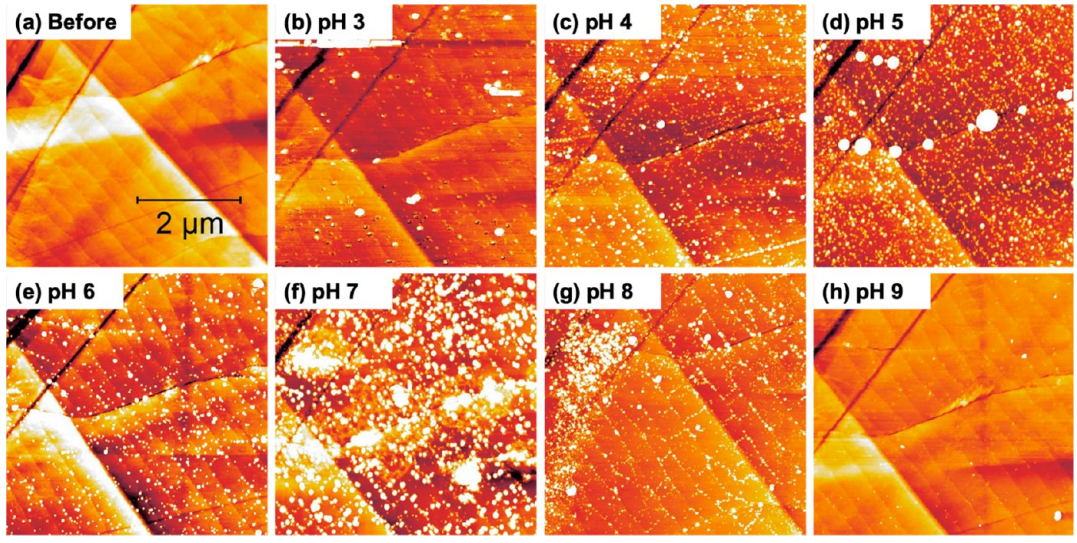

Figure 4. Topographic AFM images of the same location on a $SrTiO_3$ (110) single crystal surface (a) before and (b–h) after photochemical reaction in aqueous silver nitrate solution having pH values between pH 3–9, as indicated. The dark-to-white contrast shown is 5 nm for images a, b, and h, 10 nm for c, e, and g, and 15 nm for d and f.

https://dx.doi.org/10.1021/acsami.0c04351
ACS Appl. Mater. Interfaces 2020, 12, 23617–23626

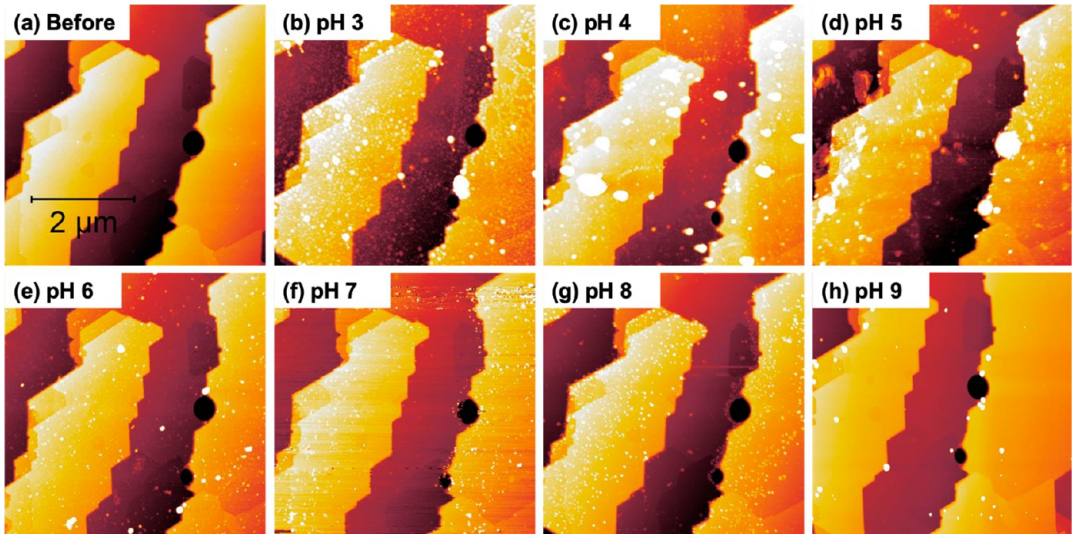

Figure 6. Topographic AFM images of the same location on a (111) $SrTiO_3$ single crystal surface (a) before and (b–h) after photochemical reaction in an aqueous silver nitrate solution having pH values between pH 3–9, as indicated. The dark-to-white contrast is 18 nm for images a, g, and h, 30 nm for b, c, and d, and 25 nm for e and f.

interpretation of the images. The observation that the reactivity maximizes at an intermediate pH is consistent with the findings for the (100) surface. However, note that the absolute photocathodic reactivity on the (110) surface is five times less than on the reactivity of the (100) surface.

The experiments carried out on the (100) and (110) surfaces were repeated on the (111) surface, and the results are shown in Figures 6 and 7. After annealing, adjacent (111)

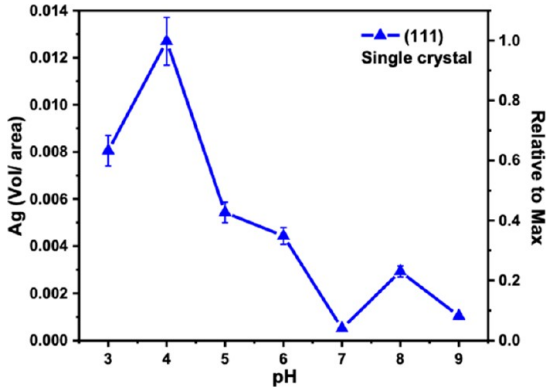

Figure 7. Excess volume of reduced Ag on the $SrTiO_3$(111) surface as a function of pH. Units are μm, computed by dividing the volume (μm^3) by the area (μm^2). The point is the mean and the bars represent the standard deviation from three measurements. The uncertainty in the silver volume is estimated to be 9%. The right-hand vertical axis quantifies the value relative to the maximum value at pH 4.

terraces are separated by a combination of straight and curved steps; the curved step edges are smaller in height than the straight ones and thus have weaker contrast in the topographic image. The formation of the reduced silver is spatially nonuniform, as reported in previous studies of the reactivity of the (111) surface.[15,32] This is related to the different chemical terminations; one of the terraces is relatively photocathodic (reduces silver) and the other is relatively photoanodic (silver is not reduced). This spatial selectivity is most obvious at pH 3 and is most clearly evident in the upper right corner of Figure 6(b). A higher resolution image illustrating the nonuniform reactivity is shown in Figure S2. Note that at pH 4, where the most silver is reduced, the surface appears to be the most uniformly reactive. The excess volume as a function of pH is illustrated Figure 7. Here, the photocathodic reactivity reaches a maximum at pH 4 and then decreases as pH increases. The absolute reactivity of the (111) surface is close to 90% of the reactivity of the (100) surface.

Parallel experiments were carried out on crystals at the surface of polycrystals. First, an orientation map was generated by EBSD (see Figure S3). Using the orientation map, it was possible to identify grains that were close to (100), (110), and (111) orientations and these grains are labeled in Figure S3. The measured deviations from the ideal orientations were 3.0°, 2.8°, and 7.6° from (100), (110), and (111), respectively. As before, the surfaces were imaged after the photoreduction of silver in solutions from pH 3 to pH 9. The results for the near (100) surface are illustrated in Figure 8, and the results for the near (110) and (111) surface are presented in Figures S4 and S5. The darkest contrast in Figure 8 corresponds to valleys at grain boundaries and residual scratches. The area on the left side of the image is near the (100) orientation. While the near (100) surface has flat (100) terraces (see Figure 8a), the surfaces near (110) and (111) have terraces that are too closely spaced to be resolved in any detail. When silver is photoreduced on the near (100) surface, it is preferentially reduced on the terraces close to an upward step. The near (110) and near (111) surfaces are so rough that it is not possible to determine if the deposits are correlated to the underlying surface structure.

A visual inspection of the images in Figure 8 indicates that there is little reactivity for the lowest and highest pH, and that the reactivity is greatest somewhere between these limits. The maximum of the height of the silver deposits is in the range of (b–d) 3–5 nm (pH 3–5), (e) 5–10 nm (pH 6), and (f–h) 1–3 nm (pH 7–9). The excess volume measurements for the (100), (110), and (111) orientations are summarized in Figure 9. For the near (100) surface, the reactivity reaches a maximum at pH 6, for the near (110) surface, the reactivity

https://dx.doi.org/10.1021/acsami.0c04351
ACS Appl. Mater. Interfaces 2020, 12, 23617–23626

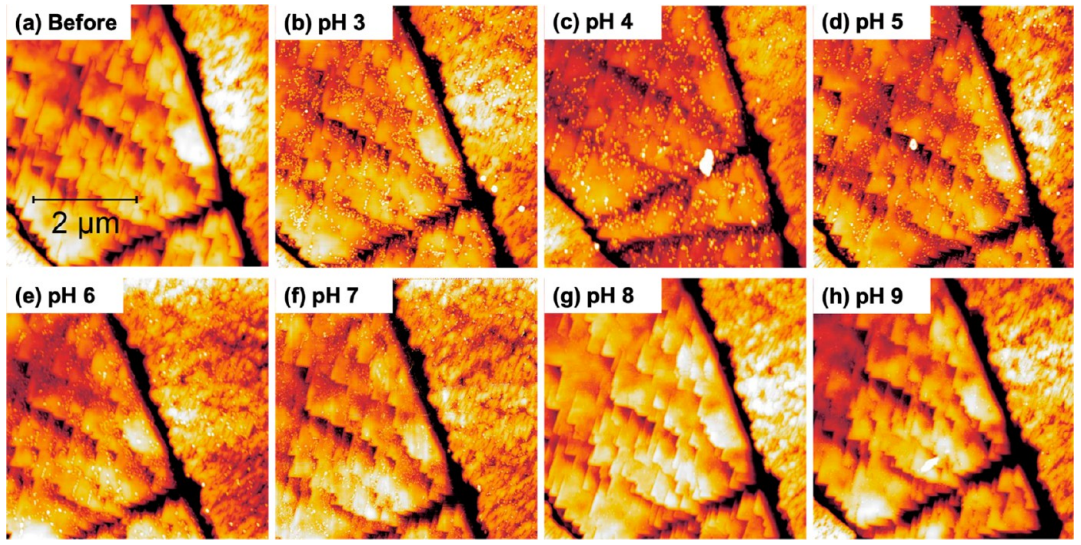

Figure 8. Topographic AFM images of the same area on a near (100) oriented grain shown in (a) before and (b–h) after photochemical reaction in an aqueous silver nitrate solution having pH values between pH 3–9, as indicated. The dark-to-white contrast in all images is 30 nm.

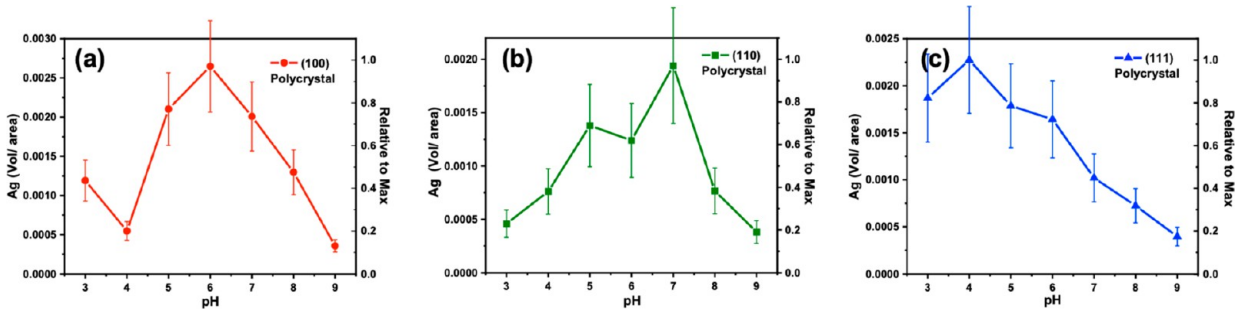

Figure 9. Excess volume as a function of pH on the polycrystalline sample for (a) the near (100) surface, (b) the near (110) surface, and (c) the near (111) surface. Units are μm, computed by dividing the volume (μm^3) by the area (μm^2). Note that the vertical scales vary in each. In each case, the point is the mean and the bars represent the standard deviation. The right-hand vertical axis quantifies the value relative to the maximum average value in each plot.

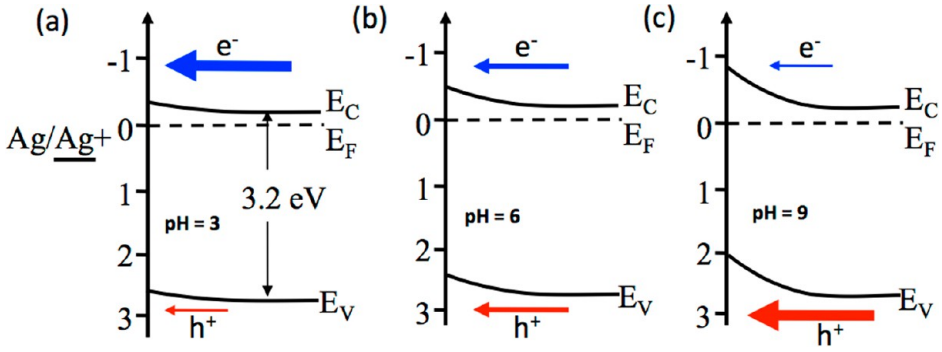

Figure 10. Schematic electronic energy levels for the bands in $SrTiO_3$. The conduction band (E_C), valence band (E_V), Fermi level (E_F), and the silver reduction potential (Ag/Ag^+) are marked. The upward band bending increases with pH. (c) At high pH, holes are more easily transported to the surface than electrons (indicated by the thickness and length of the arrows). (b) As the pH is reduced and band bending decreases, the barrier for electron transport to the surface remains, but the much higher concentration of electrons in the n-type semiconductor results in comparable electron and hole currents. (a) At the lowest pH, the overall reaction is limited by the transport of holes (minority carriers) to the surface. The energy scale is estimated based on known values for the band gap and silver reduction levels using the method outlined by Morrison.[50]

reaches a maximum at pH 7, and for the near (111) surface, the reactivity reaches a maximum at pH 4. As before, the bars represent the standard deviation of the measurements. The maxima for the reactivity of grains in polycrystals occur at the same pH as the maxima for similarly oriented single crystals. However, there is a wider range of uncertainty for the grains in the polycrystal. The increased uncertainty probably arises from the rougher surfaces, which provide steps with a variety of orientations and makes the determination of a constant background plane more uncertain. The steps also provide surfaces with different orientations that likely affect the overall reactivity.

https://dx.doi.org/10.1021/acsami.0c04351
ACS Appl. Mater. Interfaces 2020, 12, 23617–23626

DISCUSSION

The spatially selective reduction of Ag on certain terraces of the $SrTiO_3$(100) surface has not been reported previously. However, it is not too surprising. The (100) surface can be terminated by a TiO_2 or SrO layer and Paradinas et al.[48] measured a 45 mV difference between the potentials of these terraces by Kelvin probe force microscopy. Similar differences in potentials of the terraces on the (110)[16] and (111)[32] surfaces also lead to the spatially selective reduction of Ag. However, as illustrated in Figure 3b, the surface oxidizes lead with no apparent preference for a particular terrace. Therefore, the (100) surface can be considered bifunctional.

Previous observations of silver reduction on $SrTiO_3$ (at uncontrolled pH) led to the conclusion that the (100) surface is the most reactive, the (110) surface is the least reactive, and the (111) surface has an intermediate reactivity.[37] The results presented here for the single crystals are consistent with this observation (the data in Figures 2, 5, and 7 are compared on the same scale in Figure S6) for most of the pH values. However, because the pH was uncontrolled, and it is doubtful that all three surfaces have the same point of zero charge, the previous measurements were not necessarily made at the same pH. Furthermore, the photocathodic reactivity depends on the surface preparation conditions, which alters the relative coverage of photocathodic terraces.[16,32,49]

The existence of a maximum in the reactivity can be understood in terms of the surface charge. $SrTiO_3$ is an n-type semiconductor; thus, when immersed in a neutral aqueous solution, we expect a negative surface charge to develop that results in a small amount of upward band bending, as illustrated in Figure 10b. In this condition, there is a barrier for photogenerated electrons to reach the surface, while the negative surface charge will attract photogenerated holes to the surface. As established decades ago,[50] the pH of the solution alters the charge on the surface and therefore bends the bands. For example, an increase in pH makes more hydroxyl groups interact with the surface, rendering it more negative, increasing upward band bending (see Figure 10c). This will make it more difficult for electrons to get to the surface but will more strongly attract holes to the surface. If the pH decreases and more protons interact with the surface, then the surface becomes less negative (see Figure 10a). In this case, the barrier for electrons to reach the surface decreases, but holes will not be as strongly attracted to the surface (if the bands bend downward, holes will be repelled). The change in pH from 3 to 9 will lead to a change in the surface potential of 0.35 V, depicted as a change in the band edge positions from Figure 10a to 10c. With this simple picture in mind, it is easy to see how a maximum reactivity occurs at an intermediate pH. The photocathodic and photoanodic reactions are constrained by charge conservation to occur at the same rate and the overall reaction rate will therefore be limited by the slower of the two reactions. At the limit of high pH, electrons are strongly repelled from the surface, so the photocathodic reaction will limit the overall reaction rate. At the limit of low pH, holes are not as easily transported to the surface, so the photoanodic reaction will limit the overall reaction rate. It is at some intermediate pH that the maximum rate is achieved where neither reaction limits the other.

It is interesting to note that the maximum reactivity for the different surfaces is found at different values of pH. This suggests that the surfaces have different potentials. Considering the fact that the solution potential changes by ≈59 mV for each pH unit, this implies that the difference in the potential between the (111) and (110) surfaces is 0.177 V. That the different orientations of $SrTiO_3$ have different potentials is not surprising, considering the anisotropic dispersion of the valence and conduction bands.[51] Evidence for different potentials on different surface orientations of TiO_2 can be found in the work of by Bullard and Cima,[52] who found that the isoelectric points the (100), (110), and (001) surfaces vary over a range of 2.6 pH units (0.153 V). It would be interesting to compare the pH of maximum reactivity with the isoelectric point of $SrTiO_3$. Unfortunately, there is little consensus in the literature about the isoelectric point of $SrTiO_3$.[53,54] It has been reported to be pH 2.4,[55] pH 3.5,[56] pH 7.8,[57] pH 8.5,[58] pH 9.3,[59] and pH 9.5.[60] Note that we do not expect the maximum reactivity to be at the isoelectric point. Because the electrons are the majority carriers, we assume that they are abundant at the surface under most conditions. If so, it is likely that the maximum reactivity occurs under conditions where the holes are promoted to the surface by upward band bending and there is still a small barrier for the promotion of elections to the surface.

It is important to keep in mind that the pH of maximum reactivity identified in these studies is an average behavior found on a heterogeneous surface. All of the surfaces have terraces that are relatively more photocathodic or photoanodic, depending on the termination. Evidence for this can be seen in the spatial selectivity of the silver reduction. Furthermore, depending on the surface preparation, the ratio of photocathodic to photoanodic terraces will vary.[16,32] This will likely influence the isoelectric point of the surface and the pH of maximum reactivity. It is interesting to note that at pH 4, where the (111) surface has maximum reactivity, the spatial selectivity disappears, and all terraces appear equally reactive. On the contrary, at pH 6 where the (100) surface has its maximum reactivity, there are clearly terraces that prefer reduction more than others.

The interpretation presented above is relatively simple and ignores other effects that can occur in solution. For example, in the lowest pH environments, there might be a competition between Ag^+ ions and protons for surface sites. However, the observation that the pH is the same before and after the reduction reaction suggests that the reaction is still dominated by Ag^+. To test for concentration effects, some experiments have been repeated in higher concentrations of Ag^+ (0.115 M), and the reactivity trend is the same as the low concentration conditions from pH 3 to pH 6.

The results reported here have implications for the design of catalyst particles and reactor conditions. First, because a single pH must be selected for the solution, it would make sense to operate in the pH 6−7 range with particles terminated by (100) or a combination of (100) and (110) facets. In this pH range, the reactivity of the (111) surface is very low, so these facets should be avoided. On the other hand, if it were favorable to operate at pH 4, then an octahedral particle bounded by (111) surfaces only would be best. While the long-term stability of the $SrTiO_3$ surface at such a low pH is questionable, it has been shown that the photochemical properties of the $SrTiO_3$ surface were not changed by thin protective coatings of TiO_2.[61] Consistent with the results presented here, it is known that the (110) surface is relatively photoanodic compared to the (100) surface.[15,39] These two surfaces are part of the equilibrium shape of $SrTiO_3$,[40,49] and it

https://dx.doi.org/10.1021/acsami.0c04351
ACS Appl. Mater. Interfaces 2020, 12, 23617−23626

is known how to produce polyhedral particles bounded by different ratios of (100) and (110) facets.[62] Therefore, one would hypothesize that crystals with both (100) and (110) facets would have higher reactivity than a particle with only one type of facet. Our observation that, under the same reaction conditions, the polycrystal surfaces with a mixture of facets are much more reactive than the single crystals, is consistent with this idea. Additional support for this idea has been reported by Hsieh et al.[63] and Mu et al.[39] who showed that $SrTiO_3$ terminated by (100) and (110) facets produced hydrogen at a greater rate than cube-shaped crystals terminated only by (100) facets. The rate of hydrogen production might further be improved by controlling the pH in the range of 6 to 7.

CONCLUSION

In the pH range of 3 to 9, the (100), (110), and (111) surfaces of $SrTiO_3$ show a maximum photochemical reactivity for the reduction of silver from an aqueous $AgNO_3$ solution at pH 6, 7, and 4, respectively. The same maxima were found on nearly ideal single crystal surfaces and on the surfaces of grains within a polycrystal that are vicinal to the ideal orientations. The relative reactivities at the pH of maximum reactivity for the (100), (110), and (111) surfaces are 1:0.2:0.9, respectively. The change in the reactivity versus pH can be understood in relation to the surface charge created by the solution. At the lowest (highest) pH, electrons (holes) are drawn to the positively (negatively) charged surface and the overall reaction is limited by the transfer of holes (electrons) to the surface. The maximum reactivity occurs at an intermediate pH where similar concentrations of electrons and holes are at the surface so the photoanodic and photocathodic reactions can proceed at the same rate. The results can be used to optimize the photochemical reactivity of $SrTiO_3$ for H_2 production or pollutant degradation by designing particles bound by specific combinations of facets and controlling the pH in the reactor.

ASSOCIATED CONTENT

Supporting Information

The Supporting Information is available free of charge at https://pubs.acs.org/doi/10.1021/acsami.0c04351.

Details of the experimental process, additional AFM images, crystal orientation data, and a summary comparison of the data in Figure 9 (PDF)

AUTHOR INFORMATION

Corresponding Author

Gregory S. Rohrer − *Department of Materials Science and Engineering, Carnegie Mellon University, Pittsburgh, Pennsylvania 15213, United States;* orcid.org/0000-0002-9671-3034; Email: gr20@andrew.cmu.edu

Authors

Mingyi Zhang − *Department of Materials Science and Engineering, Carnegie Mellon University, Pittsburgh, Pennsylvania 15213, United States;* orcid.org/0000-0002-9996-6774

Paul A. Salvador − *Department of Materials Science and Engineering, Carnegie Mellon University, Pittsburgh, Pennsylvania 15213, United States;* orcid.org/0000-0001-7106-0017

Complete contact information is available at: https://pubs.acs.org/10.1021/acsami.0c04351

Notes

The authors declare no competing financial interest.

ACKNOWLEDGMENTS

This work was supported by the National Science Foundation under grant number DMR 1609369, and the authors acknowledge the use of the Materials Characterization Facility at Carnegie Mellon University supported by grant MCF-677785.

REFERENCES

(1) Fujishima, A.; Honda, K. Electrochemcial photolysis of water at a semiconductor electrode. *Nature* **1972**, *238* (5358), 37−38.

(2) Han, F.; Kambala, V. S. R.; Srinivasan, M.; Rajarathnam, D.; Naidu, R. Tailored titanium dioxide photocatalysts for the degradation of organic dyes in wastewater treatment: A review. *Appl. Catal., A* **2009**, *359* (1−2), 25−40.

(3) Hisatomi, T.; Kubota, J.; Domen, K. Recent advances in semiconductors for photocatalytic and photoelectrochemical water splitting. *Chem. Soc. Rev.* **2014**, *43* (22), 7520−7535.

(4) McKone, J. R.; Lewis, N. S.; Gray, H. B. Will Solar-Driven Water-Splitting Devices See the Light of Day? *Chem. Mater.* **2014**, *26* (1), 407−414.

(5) Wang, Z.; Li, C.; Domen, K. Recent developments in heterogeneous photocatalysts for solar-driven overall water splitting. *Chem. Soc. Rev.* **2019**, *48* (7), 2109−2125.

(6) Maeda, K.; Domen, K. Photocatalytic Water Splitting: Recent Progress and Future Challenges. *J. Phys. Chem. Lett.* **2010**, *1* (18), 2655−2661.

(7) Qu, Y.; Duan, X. Progress, challenge and perspective of heterogeneous photocatalysts. *Chem. Soc. Rev.* **2013**, *42* (7), 2568−2580.

(8) Spanhel, L.; Haase, M.; Weller, H.; Henglein, A. Photochemistry of colloidal semiconductors 20. surface modification and stability of strong luminescing CdS particles. *J. Am. Chem. Soc.* **1987**, *109* (19), 5649−5655.

(9) Sato, S.; White, J. M. Photo-decomposition of water over Pt-TiO_2 Catalysts. *Chem. Phys. Lett.* **1980**, *72* (1), 83−86.

(10) Li, L.; Salvador, P. A.; Rohrer, G. S. Photocatalysts with internal electric fields. *Nanoscale* **2014**, *6* (1), 24−42.

(11) Wang, X.; Xu, Q.; Li, M.; Shen, S.; Wang, X.; Wang, Y.; Feng, Z.; Shi, J.; Han, H.; Li, C. Photocatalytic Overall Water Splitting Promoted by an alpha-beta phase Junction on Ga_2O_3. *Angew. Chem., Int. Ed.* **2012**, *51* (52), 13089−13092.

(12) Yang, D.; Liu, H.; Zheng, Z.; Yuan, Y.; Zhao, J.-c.; Waclawik, E. R.; Ke, X.; Zhu, H. An Efficient Photocatalyst Structure: TiO_2(B) Nanofibers with a Shell of Anatase Nanocrystals. *J. Am. Chem. Soc.* **2009**, *131* (49), 17885−17893.

(13) Dunn, S.; Jones, P. M.; Gallardo, D. E. Photochemical growth of silver nanoparticles on c^- and c^+ domains on lead zirconate titanate thin films. *J. Am. Chem. Soc.* **2007**, *129* (28), 8724−8728.

(14) Giocondi, J. L.; Rohrer, G. S. Spatially selective photochemical reduction of silver on the surface of ferroelectric barium titanate. *Chem. Mater.* **2001**, *13* (2), 241−242.

(15) Giocondi, J. L.; Rohrer, G. S. Structure sensitivity of photochemical oxidation and reduction reactions on $SrTiO_3$ surfaces. *J. Am. Ceram. Soc.* **2003**, *86* (7), 1182−1189.

(16) Zhu, Y. S.; Salvador, P. A.; Rohrer, G. S. Controlling the termination and photochemical reactivity of the $SrTiO_3$(110) surface. *Phys. Chem. Chem. Phys.* **2017**, *19* (11), 7910−7918.

(17) Chen, F.; Huang, H. W.; Guo, L.; Zhang, Y. H.; Ma, T. Y. The Role of Polarization in Photocatalysis. *Angew. Chem., Int. Ed.* **2019**, *58* (30), 10061−10073.

(18) Inoue, Y.; Sato, K.; Sato, K.; Miyama, H. Photo assisted water decomposition by ferroelectric lead zirconate titanate ceramics with

anomalous photovoltaic effects. *J. Phys. Chem.* **1986**, *90* (13), 2809−2810.
(19) Kakekhani, A.; Ismail-Beigi, S.; Altman, E. I. Ferroelectrics: A pathway to switchable surface chemistry and catalysis. *Surf. Sci.* **2016**, *650*, 302−316.
(20) Khan, M. A.; Nadeem, M. A.; Idriss, H. Ferroelectric polarization effect on surface chemistry and photo-catalytic activity: A review. *Surf. Sci. Rep.* **2016**, *71* (1), 1−31.
(21) Li, L.; Rohrer, G. S.; Salvador, P. A. Heterostructured Ceramic Powders for Photocatalytic Hydrogen Production: Nanostructured TiO_2 Shells Surrounding Microcrystalline (Ba,Sr)TiO_3 Cores. *J. Am. Ceram. Soc.* **2012**, *95* (4), 1414−1420.
(22) Munprom, R.; Salvador, P. A.; Rohrer, G. S. Ferroelastic domains improve photochemical reactivity: a comparative study of monoclinic and tetragonal $(Bi_{1-0.5x}Na_{0.5x})(V_{1-x}Mo_x)O_4$ ceramics. *J. Mater. Chem. A* **2016**, *4* (8), 2951−2959.
(23) Zhong, Y.; Ueno, K.; Mori, Y.; Shi, X.; Oshikiri, T.; Murakoshi, K.; Inoue, H.; Misawa, H. Plasmon-Assisted Water Splitting Using Two Sides of the Same $SrTiO_3$ Single-Crystal Substrate: Conversion of Visible Light to Chemical Energy. *Angew. Chem., Int. Ed.* **2014**, *53* (39), 10350−10354.
(24) Ohtani, B.; Okugawa, Y.; Nishimoto, S.; Kagiya, T. Photocatalytic activity of TiO_2 powders suspended in aqueous silver-nitrate solution - correlation with pH-dependent surface-structures. *J. Phys. Chem.* **1987**, *91* (13), 3550−3555.
(25) Prairie, M. R.; Evans, L. R.; Stange, B. M.; Martinez, S. L. An investigation of TiO_2 photocatalysis for the treatment of water contaminated with metals and organic-chemicals. *Environ. Sci. Technol.* **1993**, *27* (9), 1776−1782.
(26) Oosawa, Y.; Gratzel, M. Enhancement of photocatalytic oxygen evolution in aqueous TiO_2 suspensions by removal of surface-OH groups. *J. Chem. Soc., Chem. Commun.* **1984**, *24*, 1629−1630.
(27) Guo, Y. X.; Siretanu, I.; Zhang, Y. H.; Mei, B.; Li, X. W.; Mugele, F.; Huang, H. W.; Mul, G. pH-Dependence in facet-selective photo-deposition of metals and metal oxides on semiconductor particles. *J. Mater. Chem. A* **2018**, *6* (17), 7500−7508.
(28) Goto, Y.; Hisatomi, T.; Wang, Q.; Higashi, T.; Ishikiriyama, K.; Maeda, T.; Sakata, Y.; Okunaka, S.; Tokudome, H.; Katayama, M.; Akiyama, S.; Nishiyama, H.; Inoue, Y.; Takewaki, T.; Setoyama, T.; Minegishi, T.; Takata, T.; Yamada, T.; Domen, K. A Particulate Photocatalyst Water-Splitting Panel for Large-Scale Solar Hydrogen Generation. *Joule* **2018**, *2* (3), 509−520.
(29) Luo, J. H.; Maggard, P. A. Hydrothermal synthesis and photocatalytic activities of $SrTiO_3$-coated Fe_2O_3 and $BiFeO_3$. *Adv. Mater.* **2006**, *18* (4), 514−517.
(30) Zhao, Z. Q.; Goncalves, R. V.; Barman, S. K.; Willard, E. J.; Byle, E.; Perry, R.; Wu, Z. K.; Huda, M. N.; Moule, A. J.; Osterloh, F. E. Electronic structure basis for enhanced overall water splitting photocatalysis with aluminum doped $SrTiO_3$ in natural sunlight. *Energy Environ. Sci.* **2019**, *12* (4), 1385−1395.
(31) Ocal, C.; Bachelet, R.; Garzon, L.; Stengel, M.; Sanchez, F.; Fontcuberta, J. Nanoscale Laterally Modulated Properties of Oxide Ultrathin Films by Substrate Termination Replica through Layer-by-Layer Growth. *Chem. Mater.* **2012**, *24* (21), 4177−4184.
(32) Zhu, Y.; Salvador, P. A.; Rohrer, G. S. Controlling the Relative Areas of Photocathodic and Photoanodic Terraces on the $SrTiO_3$(111) Surface. *Chem. Mater.* **2016**, *28* (14), 5155−5162.
(33) Song, W.; Salvador, P. A.; Rohrer, G. S. The effect of pH on the photochemical reactivity of $BaTiO_3$. *Surf. Sci.* **2018**, *675*, 83−90.
(34) Song, W.; Lopato, E. M.; Bernhard, S.; Salvador, P. A.; Rohrer, G. S. High-throughput measurement of the influence of pH on hydrogen production from $BaTiO_3/TiO_2$ core/shell photocatalysts. *Appl. Catal., B* **2020**, *269*, 118750
(35) Glickstein, J. J.; Salvador, P. A.; Rohrer, G. S. Computational Model of Domain-Specific Reactivity on Coated Ferroelectric Photocatalysts. *J. Phys. Chem. C* **2016**, *120* (23), 12673−12684.
(36) Chen, P.; Sun, Y. J.; Liu, H. J.; Zhou, Y.; Jiang, G. M.; Lee, S. C.; Zhang, Y. X.; Dong, F. Facet-dependent photocatalytic NO conversion pathways predetermined by adsorption activation patterns. *Nanoscale* **2019**, *11* (5), 2366−2373.
(37) Giocondi, J. L.; Salvador, P. A.; Rohrer, G. S. The origin of photochemical anisotropy in $SrTiO_3$. *Top. Catal.* **2007**, *44* (4), 529−533.
(38) Li, J. Y.; Dong, X. A.; Sun, Y. J.; Cen, W. L.; Dong, F. Facet-dependent interfacial charge separation and transfer in plasmonic photocatalysts. *Appl. Catal., B* **2018**, *226*, 269−277.
(39) Mu, L.; Zhao, Y.; Li, A.; Wang, S.; Wang, Z.; Yang, J.; Wang, Y.; Liu, T.; Chen, R.; Zhu, J.; Fan, F.; Li, R.; Li, C. Enhancing charge separation on high symmetry $SrTiO_3$ exposed with anisotropic facets for photocatalytic water splitting. *Energy Environ. Sci.* **2016**, *9* (7), 2463−2469.
(40) Rheinheimer, W.; Baeurer, M.; Chien, H.; Rohrer, G. S.; Handwerker, C. A.; Blendell, J. E.; Hoffmann, M. J. The equilibrium crystal shape of strontium titanate and its relationship to the grain boundary plane distribution. *Acta Mater.* **2015**, *82*, 32−40.
(41) Burbure, N. V.; Salvador, P. A.; Rohrer, G. S. Photochemical Reactivity of Titania Films on $BaTiO_3$ Substrates: Origin of Spatial Selectivity. *Chem. Mater.* **2010**, *22* (21), 5823−5830.
(42) Kalinin, S. V.; Bonnell, D. A.; Alvarez, T.; Lei, X.; Hu, Z.; Ferris, J. H.; Zhang, Q.; Dunn, S. Atomic polarization and local reactivity on ferroelectric surfaces: A new route toward complex nanostructures. *Nano Lett.* **2002**, *2* (6), 589−593.
(43) Wenderich, K.; Mul, G. Methods, Mechanism, and Applications of Photodeposition in Photocatalysis: A Review. *Chem. Rev.* **2016**, *116* (23), 14587−14619.
(44) Delahay, P.; Pourbaix, M.; Van Rysselberghe, P. Potential-pH diagram of silver - construction of the diagram - its applications to the study of the properties of the metal, its compounds, and its corrosion. *J. Electrochem. Soc.* **1951**, *98* (2), 65−67.
(45) Necas, D.; Klapetek, P. Gwyddion: an open-source software for SPM data analysis. *Cent. Eur. J. Phys.* **2012**, *10* (1), 181−188.
(46) Yam, H.; Zhang, Z. T.; Li, M.; Wang, S. H.; Ren, L. X.; Jin, K. X. Photoresponsive properties at (001), (111) and (110) $LaAlO_3$/$SrTiO_3$ interfaces. *J. Phys.: Condens. Matter* **2020**, *32* (13).
(47) Koster, G.; Kropman, B. L.; Rijnders, G.; Blank, D. H. A.; Rogalla, H. Quasi-ideal strontium titanate crystal surfaces through formation of strontium hydroxide. *Appl. Phys. Lett.* **1998**, *73* (20), 2920−2922.
(48) Paradinas, M.; Garzon, L.; Sanchez, F.; Bachelet, R.; Amabilino, D. B.; Fontcuberta, J.; Ocal, C. Tuning the local frictional and electrostatic responses of nanostructured SrTiO3-surfaces by self-assembled molecular monolayers. *Phys. Chem. Chem. Phys.* **2010**, *12* (17), 4452−4458.
(49) Pisat, A. S.; Salvador, P. A.; Rohrer, G. S. The Facet Structure and Photochemical Reactivity of Arbitrarily Oriented Strontium Titanate Surfaces. *Adv. Mater. Interfaces* **2019**, *6* (16), 1900731
(50) Morrison, S. R. *Electrochemistry at Semiconductor and Oxidized Metal Electrodes*; Plenum Press: New York, 1980.
(51) van Benthem, K.; Elsasser, C.; French, R. H. Bulk electronic structure of $SrTiO_3$: Experiment and theory. *J. Appl. Phys.* **2001**, *90* (12), 6156−6164.
(52) Bullard, J. W.; Cima, M. J. Orientation dependence of the isoelectric point of TiO_2 (rutile) surfaces. *Langmuir* **2006**, *22* (24), 10264−10271.
(53) Kosmulski, M. pH-dependent surface charging and points of zero charge. IV. Update and new approach. *J. Colloid Interface Sci.* **2009**, *337* (2), 439−448.
(54) Kosmulski, M. The pH dependent surface charging and points of zero charge. VII. Update. *Adv. Colloid Interface Sci.* **2018**, *251*, 115−138.
(55) Polli, A. D.; Wagner, T.; Ruhle, M. Effect of Ca impurities and wet chemical etching on the surface morphology of SrTiO3 substrates. *Surf. Sci.* **1999**, *429* (1−3), 237−245.
(56) Garcia-Lopez, E.; Marci, G.; Megna, B.; Parisi, F.; Armelao, L.; Trovarelli, A.; Boaro, M.; Palmisano, L. $SrTiO_3$-based perovskites: Preparation, characterization and photocatalytic activity in gas-solid regime under simulated solar irradiation. *J. Catal.* **2015**, *321*, 13−22.

https://dx.doi.org/10.1021/acsami.0c04351
ACS Appl. Mater. Interfaces 2020, 12, 23617−23626

(57) Diamant, Y.; Chen, S. G.; Melamed, O.; Zaban, A. Core-shell nanoporous electrode for dye sensitized solar cells: the effect of the $SrTiO_3$ shell on the electronic properties of the TiO_2 core. *J. Phys. Chem. B* **2003**, *107* (9), 1977−1981.
(58) Ortiz-Oliveros, H. B.; Ordonez-Regil, E.; Fernandez-Valverde, S. M. Sorption of uranium(VI) onto strontium titanate in KNO_3 medium. *J. Radioanal. Nucl. Chem.* **2009**, *279* (2), 601−610.
(59) Konstas, P.-S.; Konstantinou, I.; Petrakis, D.; Albanis, T. Development of $SrTiO_3$ Photocatalysts with Visible Light Response Using Amino Acids as Dopant Sources for the Degradation of Organic Pollutants in Aqueous Systems. *Catalysts* **2018**, *8* (11), 528
(60) Garcia-Rosales, G.; Drot, R.; Mercier-Bion, F.; Lagarde, G.; Simoni, E. Interaction between U(VI) and $SrTiO_3$ surfaces versus temperature. *J. Colloid Interface Sci.* **2009**, *333* (1), 104−113.
(61) Zhu, Y. S.; Salvador, P. A.; Rohrer, G. S. Buried Charge at the $TiO_2/SrTiO_3$ (111) Interface and Its Effect on Photochemical Reactivity. *ACS Appl. Mater. Interfaces* **2017**, *9* (8), 7843−7851.
(62) Dong, L. Q.; Shi, H.; Cheng, K.; Wang, Q.; Weng, W. J.; Han, W. Q. Shape-controlled growth of $SrTiO_3$ polyhedral submicro/nanocrystals. *Nano Res.* **2014**, *7* (9), 1311−1318.
(63) Hsieh, P. L.; Naresh, G.; Huang, Y. S.; Tsao, C. W.; Hsu, Y. J.; Chen, L. J.; Huang, M. H. Shape-Tunable $SrTiO_3$ Crystals Revealing Facet-Dependent Optical and Photocatalytic Properties. *J. Phys. Chem. C* **2019**, *123* (22), 13664−13671.

https://dx.doi.org/10.1021/acsami.0c04351
ACS Appl. Mater. Interfaces 2020, 12, 23617−23626